ChemComm

COMMUNICATION

Comparison of molecular conductance between planar and twisted 4-phenylpyridines by means of two-dimensional phase separation of tetraphenylporphyrin templates at a liquid–HOPG interface†

Takeshi Sakano, Kenji Higashiguchi and Kenji Matsuda*

Tetraphenylporphyrin (TPP) rhodium chlorides coordinated by planar and twisted 4-phenylpyridine derivatives were synthesized. An STM image was taken by a 2-D phase separation technique and the conductance was evaluated. Difference in apparent height between these phenylpyridines reflects the conductance ratio of ligands.

The investigation of single molecular conductance is a key issue in the molecular electronics field and is developing rapidly using several measurement techniques.[1] Although most experiments on the conductance of a single molecule exhibit considerable variations, the reliability of the measurements has recently been significantly increased owing to the statistical treatment by the methods of mechanically controllable break junction (MCBJ)[2] and scanning tunneling microscopy break junction (STM–BJ).[3,4]

Among several methods for the measurement of the molecular conductance, apparent height measurement by STM has the merit of applicability to many samples.[5,6] The method often utilizes the plating of target molecules into the self-assembled monolayers (SAMs) of alkanethiols on an Au substrate in order to prevent the intermolecular interaction among target molecules. However, this usual method precludes the statistical treatment because only few spots of target molecules are observable from one STM image. Use of a molecular template is one candidate to avoid the intermolecular interaction and STM observation of the SAM of samples on the templates makes the statistical analysis possible. Herein, we report on the comparison of molecular conductance between planar and twisted 4-phenylpyridine derivatives by using porphyrin templates, and show that a two-dimensional (2-D) phase separation technique is effective to discriminate these phenylpyridines on the substrate.
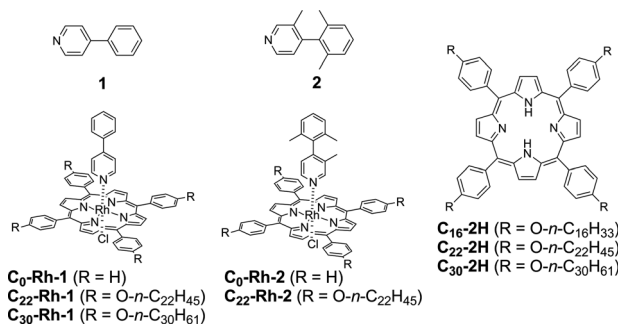
Department of Synthetic Chemistry and Biological Chemistry, Graduate School of Engineering, Kyoto University, Katsura, Nishikyo-ku, Kyoto 615-8510, Japan.
E-mail: kmatsuda@sbchem.kyoto-u.ac.jp
† Electronic supplementary information (ESI) available: Synthetic procedures of a 4-phenylpyridine derivative, TPP rhodium chlorides, ^{1}H NMR spectra of all compounds, additional STM images, details of lattice parameters, and crystallographic data of C_0-Rh-1 and C_0-Rh-2. CCDC 814313–814314. For ESI and crystallographic data in CIF or other electronic format see DOI: 10.1039/c1cc12041g

Fig. 1 Molecular structures of synthesized 4-phenylpyridines, TPPs, and TPP rhodium chlorides.

Pyridine-coordinated tetraphenylporphyrin (TPP) Rh(III) chloride having long alkyl chains forms 2-D lamellar structures at a liquid–HOPG interface, where a strongly bound axial ligand of pyridine is placed perpendicular on the TPP.[7] Therefore, TPP rhodium chloride can be used as a molecular template for the compounds carrying pyridyl groups. 4-Phenylpyridine derivatives **1** and **2** having the same molecular lengths and the different torsion angles were selected to investigate the differences in the apparent height in STM images because they are expected to have different molecular conductances due to the different torsion angles (Fig. 1).[4]

Syntheses of 4-phenylpyridine-coordinated TPP rhodium chlorides (C_0-Rh-1, C_0-Rh-2, C_{22}-Rh-1, C_{22}-Rh-2, and C_{30}-Rh-1) were carried out according to the general organic synthesis procedure described in ESI.† Subscript numbers 0, 22, and 30 show the length of alkyl side chains. Free base TPPs C_{16}-2H, C_{22}-2H, and C_{30}-2H were also synthesized. X-Ray crystallographic analysis of C_0-Rh-1 and C_0-Rh-2 revealed that the dihedral angles between the phenyl ring and the pyridyl ring of **1** and **2** are 27° and 68°, respectively. The ORTEP drawings are shown in ESI.†

STM images for a solution of C_{22}-Rh-1 and for a 1 : 1 mixed solution of C_{22}-Rh-1 and C_{22}-Rh-2 were obtained at the 1-octanoic acid–HOPG interface in the constant current mode.[8] As shown in Fig. 2a and b, both samples formed SAMs of characteristic lamellar structures, where TPPs are aligned side by side in the bright stripes. The stripes are separated by the alkyl chains from the neighboring TPP arrays.[9] In the dark areas the alkyl chains are interdigitated,

Fig. 2 STM images at the 1-octanoic acid–HOPG interface in the constant current mode: (a) C_{22}-Rh-1 (3.0×10^{-6} M) (50×50 nm^2, $I_{set} = 30$ pA, $V_{bias} = -1.0$ V); (b) a 1:1 mixed solution of C_{22}-Rh-1 (1.5×10^{-6} M) and C_{22}-Rh-2 (1.5×10^{-6} M) (60×60 nm^2, $I_{set} = 30$ pA, $V_{bias} = -1.0$ V). (c) Section analysis for the image (a). Histograms of apparent height of TPP cores: (d) for the image (a); (e) for the image (b).

although detailed structure of these chains was not observed in these images. The lattice parameters of the unit cell $a \times b$ and α were 3.9 ± 0.2 nm $\times$ 1.8 ± 0.2 nm and $71°$ for C_{22}-Rh-1 and 4.2 ± 0.2 nm $\times$ 2.3 ± 0.2 nm and $82°$ for a mixture of C_{22}-Rh-1 and C_{22}-Rh-2. These values are similar to that of characteristic lamellar structures of C_{22}-2H at the phenyloctane–HOPG interface (Fig. S3, ESI†, 4.1 ± 0.2 nm $\times$ 1.9 ± 0.2 nm and $84°$; also reported in ref. 10 as 4.2×2.1 nm and $84°$).

Contrast of the TPP core shows the apparent height of the core above the alkyl side chains. Section analysis of Fig. 2a is shown in Fig. 2c. Statistical analyses of apparent height for these STM images based on the section analysis are shown in Fig. 2d and e. Both statistical distributions of apparent heights were fitted by a single Gaussian function. By mixing C_{22}-Rh-2 into C_{22}-Rh-1, an apparent height distribution got lowered and broadened from 3.9 ± 0.5 Å to 3.6 ± 0.9 Å. In terms of apparent height, absolute values of the height are generally varied with measurement conditions even in the same setup. Therefore, the decrease of apparent height by mixing C_{22}-Rh-2 does not give the relationship of apparent height between C_{22}-Rh-1 and C_{22}-Rh-2. However, the result of broadening of the distribution suggests that C_{22}-Rh-2 shows the different apparent height from C_{22}-Rh-1. Since topographic heights are the same for C_{22}-Rh-1 and C_{22}-Rh-2 at the 1-octanoic acid–HOPG interface, this difference in apparent height shows the difference in a tunneling decay constant of axial ligands of **1** and **2**.

To clear up this difference, apparent height distributions for these two ligands need to be distinctly separated. We focused our attention on the coadsorption phenomena at a liquid–solid interface[11] and the coadsorption behavior of two free base TPPs, C_{16}-2H and C_{22}-2H, was examined. Fig. 3a shows STM images for a mixed solution of C_{16}-2H and C_{22}-2H. Two domains were observed and each domain has different lattice parameters. Lattice parameters of the right domain
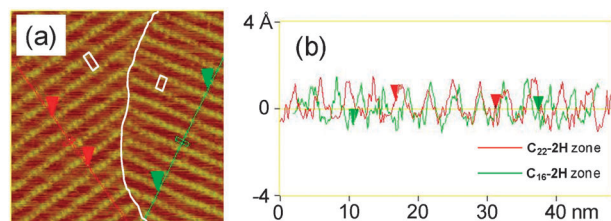

Fig. 3 STM image at the 1-phenyloctane–HOPG interface in the constant current mode: (a) a 3:1 mixed solution of C_{16}-2H (1.2×10^{-6} M) and C_{22}-2H (4.0×10^{-7} M) (50×50 nm^2, $I_{set} = 30$ pA, $V_{bias} = -1.0$ V). (b) Section analyses of C_{22}-2H (red line) and C_{16}-2H (green line) domains. White parallelograms in the STM images show the unit cells.
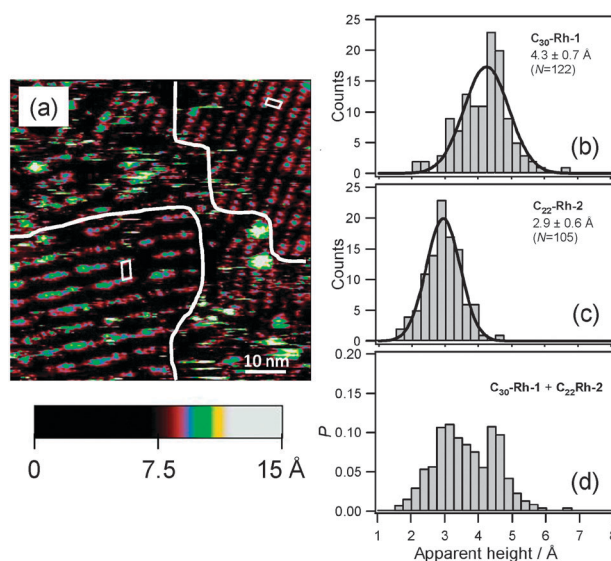

Fig. 4 (a) An STM image of a 10:1 mixed solution of C_{22}-Rh-2 (1.5×10^{-6} M) and C_{30}-Rh-1 (1.5×10^{-7} M) (75×75 nm^2, $I_{set} = 30$ pA, $V_{bias} = -1.0$ V) at the 1-octanoic acid–HOPG interface in the constant current mode. Histograms of apparent height in the domain of (b) C_{30}-Rh-1, (c) C_{22}-Rh-2, and (d) both C_{30}-Rh-1 and C_{22}-Rh-2. The contribution in counts from each domain was normalized to 1:1 in histogram (d).

were 3.4 ± 0.2 nm $\times$ 1.8 ± 0.2 nm and $89°$, whereas those of the left one were 4.0 ± 0.2 nm $\times$ 1.6 ± 0.2 nm and $88°$. These two parameters are similar to those of C_{16}-2H and C_{22}-2H. This result shows that the 2-D phase separation of C_{16}-2H and C_{22}-2H occurred at the solid–liquid interface. Section analysis of each domain shows that there is no significant difference in the apparent height, suggesting that the length of alkyl side chain does not influence the apparent height (Fig. 3b).

By means of the 2-D phase separation method, the apparent height of **1** and **2** was measured. Fig. 4a shows an STM image of a mixed solution of C_{30}-Rh-1 and C_{22}-Rh-2. Two domains having different lattice parameters of the unit cell were observed in one STM image. A domain on the bottom-left corner had a lattice spacing corresponding to that of C_{30}-2H (Fig. S3, ESI†) and another one on the upper-right corner had a similar spacing of C_{22}-2H lattice. These domains correspond to the domains of C_{30}-Rh-1 and C_{22}-Rh-2. Histograms of apparent height were separately created for each domain as shown in Fig. 4b and c. Apparent heights were obtained as 4.3 ± 0.7 Å
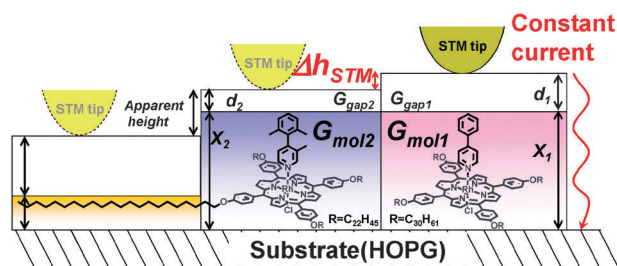
Fig. 5 Schematic drawing of the two-layer tunnel junction model for the STM measurement of a mixed solution of **C₃₀-Rh-1** and **C₂₂-Rh-2**.

for **C₃₀-Rh-1** and 2.9 ± 0.6 Å for **C₂₂-Rh-2**. Since geometrical molecular heights of **C₃₀-Rh-1** and **C₂₂-Rh-2** are the same, the difference in apparent height should originate from the conductance ratio of two ligands **1** and **2**. Summation of these histograms gave a broad distribution (Fig. 4d), which is in good agreement with the distribution of an apparent height of 1 : 1 mixture of **C₂₂-Rh-1** and **C₂₂-Rh-2** that has already been shown in Fig. 2e.

According to the two-layer tunnel junction model proposed by Weiss *et al.*,[5] the total conductance (G_{total}) between an STM tip and a substrate is described by product of the gap conductance ($G_{gap} = A \exp(-\alpha d)$) and molecular conductance ($G_{mol} = B \exp(-\beta x)$), where A and B are contact conductances, α and β are decay constants of the gap and the molecule, d is the gap distance and x is the molecular length. G_{total} is constant everywhere, therefore, the conductance ratio (G_{mol1}/G_{mol2}) is given by the following eqn (1):

$$\frac{G_{mol1}}{G_{mol2}} = \frac{G_{gap2}}{G_{gap1}} = \frac{A_2}{A_1}\exp\{\alpha(d_1 - d_2)\} \qquad (1)$$

This equation means that the ratio of A_2/A_1, decay constant of the gap (α), and difference in gap distance (d_1-d_2) give the conductance ratio. The measurement condition is identical because STM measurement was carried out for structurally similar phenylpyridines **C₃₀-Rh-1** and **C₂₂-Rh-2** and both molecules were observed in the same STM image. Therefore, contact-dependent terms A_1 and A_2 are assumed to be equal. Additionally, because x_1 and x_2 are the same, the term (d_1-d_2) is equal to the difference in apparent height Δh_{STM} (Fig. 5). Then, eqn (1) is transformed to the following simple form:

$$\frac{G_{mol1}}{G_{mol2}} = \exp\{\alpha\Delta h_{STM}\} \qquad (2)$$

This eqn (2) means that decay constant α of the gap and experimentally obtained Δh_{STM} give the conductance ratio between **C₃₀-Rh-1** and **C₂₂-Rh-2**. Since the STM measurement was conducted at the 1-octanoic acid–HOPG interface, α value of vacuum cannot be applied. We adopted the decay constant of a methylene unit ($\beta = 1.2$ Å^{-1}) reported by the measurement of a series of alkanethiols as a substitute for 1-octanoic acid.[5] By introducing the measurement result $\Delta h_{STM} = 1.4$ Å, the conductance ratio between **C₃₀-Rh-1** and **C₂₂-Rh-2** is finally obtained to be $G_{mol1}/G_{mol2} = 5.4$. Since these phenylpyridines **1** and **2** are supported by cognate templates, this conductance ratio originated from the twisting effect of the ligands. This result was compared to the $\cos^2\phi$ law proposed by Venkataraman *et al.*, in which molecular conductance of

4,4′-diaminobiphenyl is proportional to the $\cos^2\phi$, where ϕ is a dihedral angle.[4] Dihedral angles of **1** (27°) and **2** (68°) obtained from X-ray crystallographic analysis give conductance ratio $\cos^2\phi_1/\cos^2\phi_2 = 5.7$, which is in excellent agreement with experimentally obtained $G_{mol1}/G_{mol2} = 5.4$. This agreement warrants that our method is applicable to the comparison of molecular conductance.

In conclusion, we have succeeded in developing the 2-D phase separation technique of TPP templates having different lengths of side chain at a solution–HOPG interface. This technique was applied to the determination of the ratio of molecular conductance between planar and twisted phenyl-pyridines by comparing apparent height in the STM image. This technique will be the useful method for the determination of molecular conductance.

Notes and references

1 C. Joachim, J. K. Gimzewski and A. Aviram, *Nature*, 2000, **408**, 541–548; A. Nitzan and M. A. Ratner, *Science*, 2003, **300**, 1384–1389; A. Salomon, D. Cahen, S. Lindsay, J. Tomfohr, V. B. Engelkes and C. D. Frisbie, *Adv. Mater.*, 2003, **15**, 1881–1890; C. Joachim and M. A. Ratner, *Proc. Natl. Acad. Sci. U. S. A.*, 2005, **102**, 8801–8802; N. J. Tao, *Nat. Nanotechnol.*, 2006, **1**, 173–181; P. S. Weiss, *Acc. Chem. Res.*, 2008, **41**, 1772–1781; K. Moth-Poulsen and T. Bjørnholm, *Nat. Nanotechnol.*, 2009, **4**, 551–556.
2 M. A. Reed, C. Zhou, C. J. Muller, T. P. Burgin and J. M. Tour, *Science*, 1997, **278**, 252–254; M. T. Gonzalez, S. M. Wu, R. Huber, S. J. van der Molen, C. Schonenberger and M. Calame, *Nano Lett.*, 2006, **6**, 2238–2242; M. Tsutsui, M. Taniguchi, K. Yokota and T. Kawai, *Nat. Nanotechnol.*, 2010, **5**, 286–290.
3 B. Xu and N. J. Tao, *Science*, 2003, **301**, 1221–1223.
4 L. Venkataraman, J. E. Klare, C. Nuckolls, M. S. Hybertsen and M. L. Steigerwald, *Nature*, 2006, **442**, 904–907; D. Vonlanthen, A. Mishchenko, M. Elbing, M. Neuburger, T. Wandlowski and M. Mayor, *Angew. Chem., Int. Ed.*, 2009, **48**, 8886–8890; A. Mishchenko, D. Vonlanthen, V. Meded, M. Bürkle, C. Li, I. V. Pobelov, A. Bagrets, J. K. Viljas, F. Pauly, F. Evers, M. Mayor and T. Wandlowski, *Nano Lett.*, 2010, **10**, 156–163.
5 L. A. Bumm, J. J. Arnold, T. D. Dunbar, D. L. Allara and P. S. Weiss, *J. Phys. Chem. B*, 1999, **103**, 8122–8127.
6 K. Moth-Poulsen, L. Patrone, N. Stuhr-Hansen, J. B. Christensen, J.-P. Bourgoin and T. Bjørnholm, *Nano Lett.*, 2005, **5**, 783–785; S. Wakamatsu, S. Fujii, U. Akiba and M. Fujihira, *Jpn. J. Appl. Phys.*, 2006, **45**, 2736–2742.
7 J. Otsuki, *Coord. Chem. Rev.*, 2010, **254**, 2311–2341; T. Ikeda, M. Asakawa, M. Goto, K. Miyake, T. Ishida and T. Shimizu, *Langmuir*, 2004, **20**, 5454–5459.
8 UV-vis spectrum of the ligand-coordinated porphyrin in octanoic acid showed 3 nm of red-shift compared with the ligand-free porphyrin, suggesting that the pyridyl ligand is bound to the porphyrin template. See M. Hoshino, H. Seki, K. Yasufuku and H. Shizuka, *J. Phys. Chem.*, 1986, **90**, 5149–5153.
9 X. Qiu, C. Wang, Q. Zeng, B. Xu, S. Yin, H. Wang, S. Xu and C. Bai, *J. Am. Chem. Soc.*, 2000, **122**, 5550–5556; H. Wang, C. Wang, Q. Zeng, S. Xu, S. Yin, B. Xu and C. Bai, *Surf. Interface Anal.*, 2001, **32**, 266–270.
10 J. Otsuki, S. Kawaguchi, T. Yamakawa, M. Asakawa and K. Miyake, *Langmuir*, 2006, **22**, 5708–5715.
11 F. Tao, J. Goswami and S. L. Bernasek, *J. Phys. Chem. B*, 2006, **110**, 19562–19569.